Late Mesozoic exhumation of the Huangling Massif: Constraints on the evolution of the middle Yangtze River

Jianchao Su, Xu Lin, Chang'An Li, Marc Jolivet, Lin Wu, Feng Cheng, Bin Deng, Zhonghai Wu, Xiaokang Chen, Chengwei Hu

Late Mesozoic exhumation of the Huangling Massif: Constraints on the evolution of the middle Yangtze River

SU Jianchao[1], LIN Xu[2, *], LI Chang'an[1, *], Jolivet MARC [3], WU Lin[4], CHENG Feng[5], DENG Bin[6], WU Zhonghai[7], CHEN Xiaokang[2], HU Chengwei[2]

[1] *School of Geography and Information Engineering, China University of Geosciences, Wuhan 430074, China*
[2] *College of Civil Engineering and Architecture, China Three Gorges University, Yichang 443002, China*
[3] *Géosciences Rennes, CNRS-UMR6118, Univ Rennes, Rennes, France*
[4] *State Key Laboratory of Lithospheric Evolution, Institute of Geology and Geophysics, Chinese Academy of Sciences, Bejing 100029, China*
[5] *Key Laboratory of Orogenic Belts and Crustal Evolution, Ministry of Education, School of Earth and Space Sciences, Peking University, Beijing, China*
[6] *State Key Laboratory of Oil and Gas Reservoir Geology and Exploitation/Chengdu University of Technology, Chengdu, China*
[7] *Institute of Geological Mechanics, Chinese Academy of Geological Science, Beijing 100081, China*

Abstract: Plate subduction leads to complex exhumation processes on continents. The Huangling Massif lies at the northern margin of the South China Block. Whether the Huangling Massif was exhumed as a watershed of the middle reaches of the Paleo-Yangtze River during the Mesozoic remains under debate. We examined the exhumation history of the Huangling Massif based on six granite bedrock samples, using apatite fission track (AFT) and apatite and zircon (U–Th)/He (AHe and ZHe) thermochronology. These samples yielded ages of 157–132 Ma (ZHe), 119–106 Ma (AFT), and 114–72 Ma (AHe), respectively. Thermal modeling revealed that three phases of rapid cooling occurred during the Late Jurassic–Early Cretaceous, late Early Cretaceous, and Late Cretaceous. These exhumation processes led to the high topographic relief responsible for the emergence of the Huangling Massif. The integrated of our new data with published sedimentological records suggests that the Huangling Massif might have been the watershed of the middle reaches of the Paleo-Yangtze River since the Cretaceous. At that time, the rivers flowed westward into the Sichuan Basin and eastward into the Jianghan Basin. The subduction of the Pacific Plate beneath the Asian continent in the Mesozoic deeply influenced the geomorphic evolution of the South China Block.

Key words: Huangling Massif, Apatite, Zircon, (U-Th)/He, Fission track, Yangtze River

* Corresponding authors. E-mail: hanwuji-life@163.com; 1002858465@qq.com.

1 Introduction

The geomorphic evolution of a region is a direct expression of the Earth's deep dynamic action on the surface and is highly significant for understanding the relationship between tectonic deformation and surface erosion (Jolivet et al., 2010; Dong et al., 2015; Liu et al., 2015a). The Huangling Massif in northern South China is a crucial geomorphological barrier for the Yangtze River flowing into the East China Sea (Fig. 1a). Consequently, its exhumation process directly restricted the formation of the middle reaches of the Yangtze River (Richardson et al., 2010; Wang et al., 2012; Lin et al., 2022a). The formation of the 6,300-km long Yangtze River is among the most important geological events in East Asia (Zhang et al., 2008; Wang et al., 2013; Zheng et al., 2013; McPhillips et al., 2016; Wissink et al., 2016; Deng et al., 2021; Zhao et al., 2021). Therefore, the correlation between the exhumation of the Huangling Massif and the evolution of the middle reaches of the Yangtze River has attracted substantial attention. Some studies suggested that the Huangling Massif developed large rivers that flowed westward into the Sichuan Basin and eastward into the Jianghan Basin during the Mesozoic (Lee, 1924; Yang, 2006; Deng et al., 2018), indicating the existence of the Yangtze River already at this time (Fig. 1a). Conversely, some other studies pointed out that the Huangling Massif was not a watershed in which the Yangtze River flowed during the Mesozoic (Lee, 1934; Barbour, 1936). According to one model, the Yangtze River, which originates from the eastern margin of the Tibetan Plateau, flows from west to east into the Jianghan Basin (Fig. 1b) (Shen, 1965). Another model emphasizes that the Yangtze River flows from the Dabie Shan from east to west into the Sichuan Basin (Fig. 1c)(Wang et al., 2018). Consequently, whether the Huangling Massif was exhumed as a geomorphic barrier during the Mesozoic remains under debate. This also means that the development history of the middle reaches of the Yangtze River during the Mesozoic remains unclear.

In recent decades, zircon and apatite low-temperature thermochronological methods have been widely used to reconstruct the thermal histories of orogenic belts (Yu et al., 2019; Lin et al., 2021). Previous

This article has been accepted for publication and undergone full peer review but has not been through the copyediting, typesetting, pagination and proofreading process, which may lead to differences between this version and the Version of Record. Please cite this article as doi: 10.1111/1755-6724.15117.

low-temperature thermochronology studies on the Huangling Massif focused more on its Cenozoic exhumation (Richardson et al., 2010). However, the Mesozoic exhumation history of the Huangling Massif remains elusive. Here we used zircon and apatite thermochronology to constrain the Mesozoic exhumation of the Huangling Massif. Subsequently, based on the sedimentological results of the Jianghan and Sichuan Basins and the Mesozoic exhumation history of the Huangling Massif, we reconstructed the evolutionary path of the Yangtze River during the Mesozoic. Our results provide new insights to the study of the Mesozoic tectonic exhumation of the Huangling Massif and the evolution of the middle Yangtze River.

2 Geological setting

The Huangling Massif is located at the northern part of the South China Block, having an average elevation of 1,500 m and separating the Sichuan Basin to the west and the Jianghan Basin to the east (Fig. 2a). The high-grade metamorphic Archean–Paleoproterozoic Complex and Neoproterozoic granitoids are exposed in the core of the Huangling Massif (Ge et al., 2013; Wang et al., 2014). Zircon U-Pb dating indicates that granitoids of the Huangling Massif were formed between 850 and 720 Ma (Zhang et al., 2006). Its surroundings are covered and unconformably overlain by Precambrian and Phanerozoic stratigraphic rocks (Fig. 2b).

The Zigui, Dangyang, and Jianghan Basins are the main basins around the Huangling Massif (Fig. 2b)(Liu et al., 2003). Zigui Basin lies in the western Huangling Massif. Jurassic sedimentary strata are exposed in the Zigui and Dangyang Basins from the lower to the upper parts of the Tongzhuyuan (J_1t), Niejiashan (J_2n), Shaximiao (J_2s), Suining (J_3s), and Penglaizhen (J_3p) Formations (Fig. 3a)(Hubei BGMR, 1990; Liu et al., 2005). The lithology mainly consists of conglomerates, pebbled sandstone, sandstone, mudstone, locally thin limestone, and coal lines. Upper Jurassic strata are missing in the Dangyang Basin (Fig. 3b) and Jianghan Basin (Fig. 3c). Cretaceous strata are mainly distributed in the Dangyang and Jianghan Basins (Liu et al., 2015b). Lower Cretaceous strata, including the Shimen (K_1s) and Wulong (K_1w) Formations, are composed of thick conglomerates and sandstone with mudstone and muddy siltstone bands (Hubei BGMR, 1990). Upper Cretaceous strata comprise the Luojingtan (K_1l), Honghuatao (K_1h), and Paomagang (K_1p) Formations. The lithology changes from coarse conglomerates at the bottom to shale, mudstone, and marl sandstone at the top. Angular unconformity contacts between the strata occurred during the Lower Cretaceous.

3 Methods

The temperature ranges of the (U–Th)/He partial retention zones for zircon (ZHe) and apatite (AHe) are ~190–160 °C (Reiners et al., 2002) and ~70–40 °C (Farley, 2000), respectively. The apatite fission track method has closed temperatures ranging from 110 to 60 °C (Ketcham et al., 2007). Therefore, assuming a geothermal gradient of 20–25 °C/km, these low-temperature thermochronology methods can effectively reconstruct exhumation information of the upper crust over 10 km (Reiners and Brandon, 2006). Since the kinetic models of helium volume diffusion of apatite and zircon and thermal annealing of apatite fission tracks are well-established (Flowers et al., 2009), we constrain the onset of exhumation time of the Huangling Massif by thermal–kinematic modeling and an age–elevation method of the vertical profile (Fitzgerald et al., 1999; Tian et al., 2015; Lin et al., 2021).

3.1 Sampling

Six granite samples were collected from the Huangling Massif on the northern flanks of the Yangtze River (Fig. 2c). The sample locations were recorded using a handheld GPS receiver (Table 1). The surface regolith was stripped during sampling and fresh granite (~5 kg) was collected from each sampling site. The altitude of each sampling site was ~200 m.

Table 1 Metadata for the samples collected from the Huangling Massif

Sample	Rock type	Latitude	Longitude	Altitude (m)	Analyses methods
L1	Granite	30°51′86″	111°05′20″	112	ZHe, AFT, AHe
L2	Granite	30°59′24″	111°04′48″	302	ZHe, AFT, AHe
L3	Granite	31°02′24″	111°04′49″	498	ZHe, AFT, AHe
L4	Granite	31°05′25″	111°04′12″	691	ZHe, AFT, AHe
L5	Granite	31°07′12″	111°04′48″	898	ZHe, AFT, AHe
L6	Granite	31°08′24″	111°04′10″	1055	ZHe, AFT, AHe

3.2 Analytical methods

The bedrock samples collected in the field were mechanically crushed, and the apatite and zircon grains were selected through a heavy liquid and magnetic separation process. Zircon and apatite grains that were unfractured, euhedral and free of inclusions were manually selected under a microscope for subsequent (U–Th) /He dating.

The AFT ages were assessed at the Institute of Geology, China Earthquake Administration, using the laser ablation inductively coupled plasma mass spectrometry fission track (LA-ICP-MS-FT) method (Yu et al., 2019). Apatite grains were attached to the epoxy resin and polished to reveal fresh grain surfaces. Apatite spontaneous tracks were obtained by etching for 20 s at 21 °C with 5.5 M HNO_3 (Donelick et al., 1999). The horizontal confined fission tracks were obtained by measuring the track parallel to the crystallographic c-axis on the apatite surface. In general, such confined fission tracks can be used to model the thermal history of the samples; however, if their number is insufficient, the Cf-252 source can be used to increase it (Donelick and Miller, 1991). The diameter of the etched track (Dpar) was measured to assess the annealing behavior of apatite (Donelick et al., 1999). The P (χ^2) test was used to detect whether the analyzed apatite grains belonged to a single age population (Galbraith and Laslett, 1993). The specific experimental analysis process is described by Pang et al. (2017).

The selected zircon and apatite grains were digitally measured to calculate ejection corrections and then packed into niobium foil envelopes. Helium extraction, purification, and determination were performed at the (U–Th)/He laboratory at the Institute of Geology, China Earthquake Administration (Li Y et al., 2017). The apatite grains were degassed by heating with an Nd–YAG laser in a vacuum for 5 min, while the zircon grains were heated at ~1,100 °C for 10 min to to ensure extraction of 99% of He from the crystal (Li Y et al., 2017; Yu et al., 2019). Degassed apatite grains dissolved in concentrated HNO_3 and zircon grains dissolved in HF and HNO_3 were analyzed by Agilent 7900 ICP-MS to obtain the contents of U and Th. The Durango apatite and Penglai zircon were used as age standards to test the quality of the experimental analysis. Two to five apatite and zircon (U–Th)/He ages were analyzed for each sample, and Isoplot/Ex_ver3 was used to calculate the weighted mean ages (Ludwig, 2003). Apatite and zircon grain sizes (radius, Rs) and effective uranium (eU) concentration were evaluated as indicators of radiation damage (Reiners and Farley, 2001; Shuster et al., 2006).

We used the QTQt software (v 5.8.0; Gallagher, 2012) to simulate the time–temperature (t–T) thermal history of the newly acquired data to constrain the exhumation history of the Huangling Massif. QTQt extracts time–temperature paths using a Bayesian Transdimensional Markov Chain Monte Carlo inversion (Charvin et al., 2009; Gallagher, 2012; Vermeesch and Tian, 2014). This thermal history modeling method allows the simultaneous simulation of multiple thermochronometers and samples. The preset constraints before modeling were as follows: The current temperature was set to 10 ± 10 °C, the default paleogeothermal gradient was set to 30 ± 15 °C/km, with the lapse rate being 6 ± 3 °C/km, and the temperature offset was permitted to vary over time because of the instability of the paleogeothermal gradient. All model runs involved 200,000 iterations for burn-in and post-burn-in to obtain a stable result.

4 Results

4.1 Apatite fission track dating

In total, 202 analytical results were obtained for the study area (Table 2). All P(χ^2) tests exceeded 20%, indicating that only one age population was present in these samples (Fig. 4)(Galbraith, 1990). Therefore, the apatite fission-track pool ages were reported. The pool ages obtained for the six bedrock samples in reference to a vertical profile from 1,055 to 112 m elevation range from 118.7 ± 3.1 to 105.6 ± 2.2 Ma (Fig. 5). The average track length ranges from 12.69 ± 0.1 to 11.44 ± 0.2 μm, with standard deviations ranging from 1.81 to 1.56 μm (Table 1). The track-length distribution histograms exhibit a unimodal distribution pattern (Fig. 6a–f)(Gleadow et al., 1986). The Dpar values vary from 2.01 ± 0.14 to 1.85 ± 0.17 μm, thereby exhibiting no clear relationships with the corresponding apatite fission-track ages and lengths (Fig. 6g–h). This indicates that the effect of the heterogeneity of apatite grains on the annealing kinetics is minimal.

Table 2 Apatite fission-track and apatite and zircon (U–Th)/He ages

Sample No.	Nc	Dispersion %	$P(\chi^2)$ %	Fission track age (Ma ± 1σ)	MTL (μm ± 1σ) (Nj)	Standard Deviation	Dpar (μm ± SD)	AHe age (Ma ± 1σ)	ZHe age (Ma ± 1σ)
L1	34	26	44	118.7 ± 3.1	12.2 ± 0.2 （102）	1.81	1.90 ± 0.14	76.95 ± 13.70	143.50 ± 12.44
L2	34	3.7	41	118.4 ± 2.9	12.32 ± 0.2 （107）	1.61	2.01 ± 0.14	71.77 ± 4.28	135.90 ± 3.01
L3	33	0	92	112.8 ± 2.4	12.69 ± 0.1 （110）	1.56	1.85 ± 0.17	82.29 ± 9.10	157.21 ± 14.93
L4	32	0	85	117.9 ± 3.3	12.49 ± 0.2 （112）	1.64	1.87 ± 0.16	84.84 ± 7.66	132.31 ± 4.91
L5	36	0	89	105.6 ± 2.2	12.65 ± 0.1 （115）	1.58	1.89 ± 0.10	95.53 ± 9.94	141.76 ± 5.15
L6	33	5.3	21	114.8 ± 2.6	11.44 ± 0.2 （113）	1.67	1.92 ± 0.19	114.26 ± 8.10	141.11 ± 13.57

Nc = number of apatite crystals analyzed; MTL = mean confined track length; SD = standard deviation; Dpar = fission track etch pit diameter; Apatite-Zeta NIST610 = 1940 ± 50.

4.2 Apatite and zircon (U-Th)/He dating

The apatite and zircon (U–Th)/He ages are presented in Table 1. The raw data are presented in Supplementary Table S1. The weighted mean apatite (U–Th)/He age ranges from 114.26 ± 8.10 to 71.77 ± 4.28 Ma, exhibiting a marked correlation with sample elevation (Fig. 5). However, this age–elevation correlation is not evident in the zircon (U–Th)/He age range between 157.21 ± 14.93 and 132.31 ± 4.91 Ma. There are no correlations between age–eU and age–Rs were found (Fig. 7), indicating that the effect of radiation damage was not significant (Flowers et al., 2009).

4.3 Thermal modeling

We jointly modeled the zircon and apatite (U–Th)/He, and apatite fission-track ages of each sample (Fig. 8). Inverse modeling for the zircon (U–Th)/He ages indicated that the samples passed through the partial retention zone (PRZ), constraining the onset of rapid cooling events since the Late Jurassic and Early Cretaceous. Inverse modeling of the apatite fission-track ages revealed reheating from ~140 to ~130 Ma and passing through the partial annealing zone (PAZ) with monotonic cooling (Fig. 8). The inverse modeling suggested that these samples passed rapidly through the PAZ and that the onset of rapid cooling began during the late Early Cretaceous (130–120 Ma). The modeling of apatite (U–Th)/He data confirmed the rapid phase of a monotonic cooling event during the Late Cretaceous (80–70 Ma).

5 Discussion

The ZHe, AHe, and AFT ages obtained from this analysis are significantly younger than the crystallization age of the Huangling Massif (850–720 Ma; Zhang et al., 2006). This suggests that these low-temperature thermochronology ages are the times of post-crystallization cooling through the zircon and apatite PRZ and apatite PAZ during regional exhumation events. Combined with our thermal modeling results and other data from the region, three phases of cooling/exhumation events occurred from the Late Jurassic–Early Cretaceous to the Late Cretaceous in the Huangling Massif.

5.1 Late Jurassic–Early Cretaceous exhumation

The first phase of exhumation of the Huangling Massif started at 157–132 Ma, in accordance with previous zircon and apatite fission track results (150–129 Ma) reported by Ge et al., 2013 (Fig. 9a). This period was characterized by Pacific Plate subduction beneath the South China Block (Fig. 9b)(Li et al., 2014; Chu et al., 2020; Liu et al., 2021; Cao et al., 2021). Slab-triggered upper mantle upwelling was synchronous with orogenic shortening deformation and metamorphism under a NW–SE compressional setting from the South China Block (Lin et al., 2000; Liu et al., 2015a; Ji et al., 2017a; Liu et al., 2017; Gan et al., 2020). Accompanying exhumation occurred at the Xuefeng Shan (155–123 Ma; Ge et al., 2016; Chu et al., 2019), Heng Shan (150–136 Ma; Li et al., 2013, 2016a), Qinling Shan (156–124 Ma; Heberer et al., 2014; Chen et al., 2015; Wang M et al., 2022), Daba Shan (140–125 Ma; Shi et al., 2012; Tian et al., 2012; Zhang et al., 2013), Mufu Shan (150–136 Ma; Lin et al., 2000; Li et al., 2016b; Ji et al., 2017a, 2018; Shen et al., 2020) and Dabie Shan (145–125 Ma; Ratschbacher et al., 2000; Grimmer et al., 2002; Hu et al., 2006b; Ji et al., 2017b). The left-lateral strike–slip motion along the NE–SW direction during this time was accommodated on the Tanlu Fault east of the Qinling–Dabie Shan (Fig. 2a)(Ratschbacher et al., 2000; Hacker et al., 2004; Li et al., 2019). In addition, an angle unconformity between the Upper Jurassic and Lower Cretaceous strata occurred in the Zigui (Wang et al., 2012; Chai et al., 2020), Dangyang (Shi et al., 2013), and Jianghan (Shen et al., 2012a) Basins due to the rapid exhumation of the Huangling Massif. These strata are dominated by coarse clastic deposits, indicating a proximate source accumulation. Such angular unconformities and coarse-grained are also widespread in

the Sichuan (Li Y et al., 2018), Hengyang (Li et al., 2014; Dong et al., 2015), Yuanma (Li et al., 2012), and Dongting (Lin et al., 2023a) Basins within the South China Block. The Huangling Massif was involved in a series of folds with nearly N–S axes during the Early Cretaceous (Ji et al., 2014). At that time, although the Lhasa Terrane subducted from south to north beneath the southern margin of the Asian continent, the influence of the far-field effect of the subduction on the exhumation of the Huangling Massif can be ruled out (Li et al., 2014; Liu et al., 2017; Chu et al., 2020). Thus, our new low-temperature thermochronology data provide the timing of the syn-collisional exhumation of the Huangling Massif in response to the Pacific Plate subduction during the Late Jurassic–Early Cretaceous.

5.2 Late Early Cretaceous exhumation

The second phase of deformation of the Huangling Massif was marked by an abrupt exhumation starting at 119–106 Ma. Bedrock $^{40}Ar/^{39}Ar$ analyses and thermal history modeling revealed that the Huangling Massif underwent exhumation at 110 Ma (Fig. 9a)(Ji et al., 2014). Recent sedimentary evidence also supports that the Huangling Massif experienced exhumation during the late Early Cretaceous. A thick stratal succession of the Wulong Formation conglomerate deposited in the Dangyang (Shi et al., 2013) and Jianghan (Shen et al., 2012b) Basins marks the significant denudation of the Huangling Massif during this time (Fig. 3 b, c). The western Pacific oceanic plate forward subduction under East Asia occurred during the late Early Cretaceous period (Liu et al., 2005; Li et al., 2014; Liu et al., 2017; Chu et al., 2019; Li et al., 2019; Cao et al., 2021). Consequently, the NW–SE transpressional event lasting from 117 to 108 Ma caused extensive ductile–brittle deformation at the eastern margin and center of the South China Block (Li et al., 2014; Liu et al., 2017; Chu et al., 2019). More low-temperature thermochronology results show that Daba Shan (Fig. 10a)(110 Ma; Tian et al., 2012; Li W et al., 2017), Qinling–Dabie Shan (110 Ma; Grimmer et al., 2002; Hu et al., 2006b; Heberer et al., 2014; Wang et al., 2015; Wang M et al., 2022), Mufu Shan (120 Ma; Lin et al., 2000; Ji et al., 2018; Shen et al., 2020), and Xuefeng Shan (100 Ma; Chu et al., 2020), as well as the eastern Sichuan Basin (100 Ma; Shi et al., 2016), experienced rapid exhumation again in the late Early Cretaceous. Therefore, the exhumation of the Huangling Massif was spatially synchronized with the aforementioned orogenic belts.

5.3 Late Cretaceous exhumation

From an ~1-km high vertical profile with ages decreasing from 114 Ma at the peak to 77 Ma at the foot (Fig. 6), combined with the QTQt thermal modeling (Fig. 8), the age–elevation relationship suggests that the third phase of rapid exhumation of the Huangling Massif occurred during the Late Cretaceous. Apatite fission-track ages from the Huangling Massif indicate that regional exhumation occurred at 102–87 Ma (Hu et al., 2006a). Molasse deposits (Luojingtan Formation) along the periphery of the Dangyang and Jianghan Basins in the Late Cretaceous reflect this denudation (Shen et al., 2012a,b; Shi et al., 2013). A similar exhumation during the Late Cretaceous has also been proposed around the Huangling Massif. To the north, bedrock zircon and apatite (U–Th)/He and apatite fission-track ages indicate that the rapid exhumation of the Qinling–Dabie Shan occurred at 78–71 Ma (Fig. 9a)(Chen et al., 2015; Ding et al., 2021; Wang M et al., 2022). To the south, apatite fission-track and apatite (U–Th)/He ages imply that the rapid exhumation of Xuefeng Shan and Mufu Shan occurred at 84–70 Ma (Tang et al., 2014; Ge et al., 2016) and 100–80 Ma (Lin et al., 2000; Ji et al., 2018), respectively. To the west, AFT and (U–Th)/He results reveal rapid exhumation events of the eastern margin of the Sichuan Basin since 80–70 Ma (Deng et al., 2013; Shi et al., 2016; Yang et al., 2017). During the Late Cretaceous, the rollback subduction of the Pacific Plate underneath the South China Block resulted in intense extension overprinting the pre-existing shortening structures (Li et al., 2014; Liu et al., 2017; Li et al., 2019; Zhang et al., 2023). Therefore, the Huangling Massif and its surrounding orogenic belts appeared in the third phase of exhumation related to regional extension triggered by the Pacific Plate subduction.

5.4 Implications for the evolution of the middle Yangtze River

The Cretaceous tectonic evolution of South China involved alternating contractions and extensions (Chu et al., 2012; Li et al., 2014; Shi et al., 2015; Liu et al., 2017; Li J et al., 2018). In addition to the exhumation mentioned above, at least two episodes of crustal extension at 140–120 and 110–80 Ma have been identified by studies on South China (e.g., Chu and Lin, 2014; Li et al., 2014; Liu et al., 2017). The extension led to widespread generations of basins, grabens, and extensional domes, accompanied by extensive magmatism (Lin et al., 2000; Zhou et al., 2006; Shi et al., 2013; Li et al., 2014; Dong et al., 2015; Ji et al., 2018). Therefore, the exhumation of orogenic belts and the alternate emergence of extensional basins lead to prominent differences in topography, which were conducive to the development of large rivers.

The Huangling Massif experienced significant three-phase tectonic exhumation processes during the Late Mesozoic. From the Early to Late Cretaceous, molasse accumulation and fluvial–lacustrine strata were widely distributed in the Dangyang (Shi et al., 2013) and Jianghan (Shen et al., 2012a) Basins at the eastern Huangling Massif. Detrital zircon U–Pb age spectrum correlation and sedimentological evidence indicate that the Mesozoic sediments in the western Jianghan Basin mainly originated from the

Qinling Shan, Huangling Massif, and Wuling Shan (Fig. 10) (Liu et al., 2003; Shen et al., 2012a; Wang et al., 2012). Recently, Lin et al. (2023a) conducted a systematic provenance tracking study on Mesozoic strata in the western Jianghan Basin. Their results showed that these materials mainly originated from adjacent source areas and had no connection with the upper Yangtze River. Furthermore, molasse deposits developed in the eastern part of the Jianghan Basin, whereas extensive lacustrine deposits appeared in its interior (Hubei BGMR, 1990). Meanwhile, provenance tracking results from boreholes in the Yangtze River Delta (Liu et al., 2022) and East China Sea Basin (Fu et al., 2022) indicate that large flowing rivers did not exist in the Cretaceous. This shows that there was no modern Yangtze River in the eastern Huangling Massif in the Cretaceous. In contrast, the detrital zircon U–Pb age spectra and analysis of heavy minerals and sedimentary facies suggest that a large river connected the western Huangling Massif, Sichuan Basin, Chuxiong Basin, and Lanping Basin during the Cretaceous (Deng et al., 2018; Wang L et al., 2022; Wang et al., 2023; Zhao et al., 2022). The lack of Cretaceous strata in the western part of the Huangling Massif and the interior of the Three Gorges (Chai et al., 2020) may be related to the outflow of the Paleo-Yangtze River. Because of the subduction of the Pacific Plate beneath the Asian continent, the topography of the South China Block was higher in the east and lower in the west from the Late Jurassic to the Late Cretaceous (Li et al., 2014; Chu et al., 2019). In addition, the Tibetan Plateau was exhumed due to the collision between the Lhasa Terrane and Asian continent during the Cretaceous (Hu et al., 2012; Zhu et al., 2013; Jolivet, 2017; Liu-Zeng et al., 2018; Yuan et al., 2021; Lin et al., 2022b, 2023b), thereby constraining the southward flow of the Paleo-Yangtze River. Therefore, it can be inferred that the Paleo-Yangtze River flew between the Tibetan Plateau and South China Block (Plateau). This pattern of river evolution is similar to that of the present-day Mississippi River in North America, which originates from the Rocky Mountains to the west and Appalachian Mountains to the east (Clark et al., 2004). Therefore, the Huangling Massif developed into a regional watershed during the Cretaceous, and the Paleo-Yangtze River did not flow through it (Figure 10).

6 Conclusions

Based on thermochronometric data (AHe, AFT, and ZHe) and thermal history modeling of the Huangling Massif (Central China), three exhumation phases were identified. The first exhumation phase started at 157–132 Ma, the subsequent exhumation phases was constrained to 119–106 Ma, and the final exhumation phase began at 77 Ma. These rock exhumations along the Huangling Massif appear to be consistent with the deformation produced by the subduction of the Pacific Plate beneath the Asian continent. Combined with the sedimentological findings obtained for the Zigui, Dangyang, and Jianghan Basins, the Huangling Massif developed into a geomorphic barrier during the Cretaceous. During this time, large rivers flowed into the Sichuan Basin on the west side of the Huangling Massif, whereas smaller rivers flowed into the Jianghan Basin on the east side. Therefore, the Paleo-Yangtze River did not flow through the Huangling Massif from east to west or west to east at this stage.

Acknowledgments

We would like to thank Dr. Li Jianhua of the Institute of Geomechanics, Chinese Academy of Sciences for the revision of the first draft of this article. This work was financially supported by the National Natural Science Foundation of China (Grants numbers 41671011; 41871019; 41877292; 41972212), Research Foundation of Chutian Scholars Program of Hubei Province (No. 8210403), and Shanxi Key Research and Development program: Feng Cheng (No. 2021SF2-03). We would like to thank Editage (www.editage.cn) for English language editing.

Reference

Barbour, G. B. 1936. Physiographic history of the Yangtze. The Geographical Journal, 87(1): 17-32.
Cao, X., Flament, N., Li, S., Müller, R. D. 2021. Spatio-temporal evolution and dynamic origin of Jurassic-Cretaceous magmatism in the South China Block. Earth-Science Reviews, 217: 103605.
Charvin, K., Gallagher, K., Hampson, G. L., Labourdette, R. 2009. A Bayesian approach to inverse modelling of stratigraphy, part 1: method. Basin Research, 21(1): 5-25.
Chai, R., Yang, J., Du, Y., Liu, J., He, F., Huang, Y., Dai, X. 2020. Constraints on the early Mesozoic denudation of the Qinling orogen from Upper Triassic-Lower Jurassic successions in the Zigui Basin, central China. Journal of Asian Earth Sciences, 195: 104360.
Chen, H., Hu, J., Wu, G., Shi, W., Geng, Y., Qu, H. 2015. Apatite fission-track thermochronological constraints on the pattern of late Mesozoic–Cenozoic uplift and exhumation of the Qinling Orogen, central China. Journal of Asian Earth Sciences, 114: 649-673.
Chu, Y., Faure, M., Lin, W., Wang, Q. 2012. Early Mesozoic tectonics of the South China block: Insights from the Xuefengshan intracontinental orogen. Journal of Asian Earth Sciences, 61: 199-220.
Chu, Y., Lin, W. 2014. Phanerozoic polyorogenic deformation in southern Jiuling Massif, northern South China block: Constraints from structural analysis and geochronology. Journal of Asian Earth Sciences, 86: 117-130.
Chu, Y., Lin, W., Faure, M., Xue, Z., Ji, W., Feng, Z. 2019. Cretaceous episodic extension in the south China block, east Asia: Evidence from the Yuechengling massif of central south China. Tectonics, 38(10): 3675-3702.
Chu, Y., Lin, W., Faure, M., Allen, M. B., Feng, Z. 2020. Cretaceous exhumation of the Triassic intracontinental

Xuefengshan Belt: Delayed unroofing of an orogenic plateau across the South China Block?. Tectonophysics, 793: 228592.
Clark, M. K., Schoenbohm, L. M., Royden, L. H., Whipple, K. X., Burchfiel, B. C., Zhang, X., Chen, L. 2004. Surface uplift, tectonics, and erosion of eastern Tibet from large- scale drainage patterns. Tectonics, 23(1): 1-21.
Deng, B., Liu, S. G., Li, Z. W., Jansa, L. F., Liu, S., Wang, G. Z., Sun, W. 2013. Differential exhumation at eastern margin of the Tibetan Plateau, from apatite fission-track thermochronology. Tectonophysics, 591: 98-115.
Deng, B., Chew, D., Jiang, L., Mark, C., Cogné, N., Wang, Z., Liu, S. 2018. Heavy mineral analysis and detrital U-Pb ages of the intracontinental Paleo-Yangzte basin: Implications for a transcontinental source-to-sink system during Late Cretaceous time. GSA Bulletin, 130(11-12): 2087-2109.
Deng, B., Chew, D., Mark, C., Liu, S., Cogné, N., Jiang, L., Li, J. 2021. Late Cenozoic drainage reorganization of the paleo-Yangtze river constrained by multi-proxy provenance analysis of the Paleo-lake Xigeda. GSA Bulletin, 133(1-2): 199-211.
Ding, R., Chang, Y., Min, K., Xu, C., Wang, W. 2021. Post-orogenic topographic evolution of the Dabie orogen, Eastern China: Insights from apatite and zircon (U-Th)/He thermochronology. Geomorphology, 374: 107487.
Donelick, R. A., Miller, D. S. 1991. Enhanced TINT fission track densities in low spontaneous track density apatites using 252Cf-derived fission fragment tracks: A model and experimental observations. International Journal of Radiation Applications and Instrumentation. Part D. Nuclear Tracks and Radiation Measurements, 18(3): 301-307.
Donelick, R. A., Ketcham, R. A., Carlson, W. D. 1999. Variability of apatite fission-track annealing kinetics: II. Crystallographic orientation effects. American Mineralogist, 84(9): 1224-1234.
Dong, S., Zhang, Y., Zhang, F., Cui, J., Chen, X., Zhang, S., Li, H. 2015. Late Jurassic–Early Cretaceous continental convergence and intracontinental orogenesis in East Asia: A synthesis of the Yanshan Revolution. Journal of Asian Earth Sciences, 114: 750-770.
Farley, K. A. 2000. Helium diffusion from apatite: General behavior as illustrated by Durango fluorapatite. Journal of Geophysical Research: Solid Earth, 105(B2): 2903-2914.
Flowers, R. M., Ketcham, R. A., Shuster, D. L., Farley, K. A. 2009. Apatite (U–Th)/He thermochronometry using a radiation damage accumulation and annealing model. Geochimica et Cosmochimica acta, 73(8): 2347-2365.
Fitzgerald, P. G., Muñoz, J. A., Coney, P. J., Baldwin, S. L. 1999. Asymmetric exhumation across the Pyrenean orogen: implications for the tectonic evolution of a collisional orogen. Earth and Planetary Science Letters, 173(3): 157-170.
Fu, X., Yang, R., Zhu, W., Yang, S., Geng, J., Zhang, L. 2022. Initiation of a “lost” large river on the East Asia margin in the Middle Eocene. Preprints.org: 1-28.
Galbraith, R. F. 1990. The radial plot: graphical assessment of spread in ages. International Journal of Radiation Applications and Instrumentation. Part D. Nuclear Tracks and Radiation Measurements, 17(3): 207-214.
Galbraith, R. F., Laslett, G. M. 1993. Statistical models for mixed fission track ages. Nuclear tracks and radiation measurements, 21(4): 459-470.
Gallagher, K. 2012. Transdimensional inverse thermal history modeling for quantitative thermochronology. Journal of Geophysical Research: Solid Earth, 117(B2): 1-16.
Gan, C., Wang, Y., Barry, T. L., Zhang, Y., Qian, X. 2020. Spatial and temporal influence of Pacific subduction on South China: geochemical migration of Cretaceous mafic–intermediate rocks. Journal of the Geological Society, 177(5): 1013-1024.
Ge, X., Shen, C., Yang, Z., Mei, L., Xu, S., Peng, L., Liu, Z. 2013. Low-temperature thermochronology constraints on the Mesozoic-Cenozoic exhumation of the Huangling massif in the Middle Yangtze Block, Central China. Journal of Earth Science, 24(4): 541-552.
Ge, X., Shen, C., Selby, D., Deng, D., Mei, L. 2016. Apatite fission-track and Re-Os geochronology of the Xuefeng uplift, China: Temporal implications for dry gas associated hydrocarbon systems. Geology, 44(6): 491-494.
Gleadow, A. J., Duddy, I. R., Green, P. F., Lovering, J. F. 1986. Confined fission track lengths in apatite: a diagnostic tool for thermal history analysis. Contributions to Mineralogy and Petrology, 94: 405-415.
Grimmer, J. C., Jonckheere, R., Enkelmann, E., Ratschbacher, L., Hacker, B. R., Blythe, A. E., Dong, S. 2002. Cretaceous-Cenozoic history of the southern Tan-Lu fault zone: apatite fission-track and structural constraints from the Dabie Shan (eastern China). Tectonophysics, 359(3-4): 225-253.
Hacker, B. R., Ratschbacher, L., Liou, J. G. 2004. Subduction, collision and exhumation in the ultrahigh-pressure Qinling-Dabie orogen. Geological Society, London, Special Publications, 226(1): 157-175.
Heberer, B., Anzenbacher, T., Neubauer, F., Genser, J., Dong, Y., Dunkl, I. 2014. Polyphase exhumation in the western Qinling Mountains, China: Rapid Early Cretaceous cooling along a lithospheric-scale tear fault and pulsed Cenozoic uplift. Tectonophysics, 617: 31-43.
Hu, S., Raza, A., Min, K., Kohn, B. P., Reiners, P. W., Ketcham, R. A., Gleadow, A. J. 2006a. Late Mesozoic and Cenozoic thermotectonic evolution along a transect from the north China craton through the Qinling orogen into the Yangtze craton, central China. Tectonics, 25(6): 1-15.
Hu, S., Kohn, B. P., Raza, A., Wang, J., Gleadow, A. J. 2006b. Cretaceous and Cenozoic cooling history across the ultrahigh pressure Tongbai–Dabie belt, central China, from apatite fission-track thermochronology. Tectonophysics, 420(3-4): 409-429.
Hu, X., Sinclair, H. D., Wang, J., Jiang, H., Wu, F. 2012. Late Cretaceous- Palaeogene stratigraphic and basin evolution in the Zhepure Mountain of southern Tibet: Implications for the timing of India- Asia initial collision. Basin research, 24(5), 520-543.
Hubei BGMR (Bureau of Geology and Mineral Resources of Hubei). 1990. Regional geology of Hubei Province. Geological Publishing House: Beijing, China, 1-705(in Chinese with English abstract).
Hubei BGMR (Bureau of Geology and Mineral Resources of Hubei).1970. 1:200000 Geological Map of China. Geological Publishing House: Beijing, China, 1.(in Chinese with English abstract).
Ji, W., Lin, W., Faure, M., Chu, Y., Wu, L., Wang, F., Wang, Q. 2014. Origin and tectonic significance of the Huangling massif within the Yangtze craton, South China. Journal of Asian Earth Sciences, 86: 59-75.
Ji, W., Lin, W., Faure, M., Chen, Y., Chu, Y., Xue, Z. 2017a. Origin of the Late Jurassic to Early Cretaceous peraluminous granitoids in the northeastern Hunan province (middle Yangtze region), South China: Geodynamic implications for the Paleo-Pacific subduction. Journal of Asian Earth Sciences, 141: 174-193.
Ji, W., Lin, W., Faure, M., Shi, Y., Wang, Q. 2017b. The early Cretaceous orogen-scale Dabieshan metamorphic core complex: implications for extensional collapse of the Triassic HP–UHP orogenic belt in east-central China. International Journal of Earth Sciences, 106: 1311-1340.

Ji, W., Faure, M., Lin, W., Chen, Y., Chu, Y., Xue, Z. 2018. Multiple emplacement and exhumation history of the Late Mesozoic Dayunshan–Mufushan batholith in southeast China and its tectonic significance: 1. Structural analysis and geochronological constraints. Journal of Geophysical Research: Solid Earth, 123(1): 689-710.
Jolivet, M., Dominguez, S., Charreau, J., Chen, Y., Li, Y., Wang, Q. 2010. Mesozoic and Cenozoic tectonic history of the central Chinese Tian Shan: Reactivated tectonic structures and active deformation. Tectonics, 29(6): 1-30.
Jolivet, M. 2017. Mesozoic tectonic and topographic evolution of Central Asia and Tibet: a preliminary synthesis. Geological Society, London, Special Publications, 427(1): 19-55.
Ketcham, R. A., Carter, A., Donelick, R. A., Barbarand, J., Hurford, A. J. 2007. Improved modeling of fission-track annealing in apatite. American Mineralogist, 92(5-6): 799-810.
Lee, J.S. 1924. Geology of the gorge district of the Yangtze (from Ichang to Tzekuei) with special reference to the development of the gorges. Bull Geol Soc China, 3: 351-391.
Lee, C. Y. 1934. The development of the upper Yangtze valley. Bull Geol Soc China, 3: 107-118.
Li, J., Zhang, Y., Dong, S., Li, H. 2012. Late Mesozoic–Early Cenozoic deformation history of the Yuanma Basin, central South China. Tectonophysics, 570: 163-183.
Li, J., Zhang, Y., Dong, S., Su, J., Li, Y., Cui, J., Shi, W. 2013. The Hengshan low-angle normal fault zone: Structural and geochronological constraints on the Late Mesozoic crustal extension in South China. Tectonophysics, 606: 97-115.
Li, J., Zhang, Y., Dong, S., Johnston, S. T. 2014. Cretaceous tectonic evolution of South China: A preliminary synthesis. Earth-Science Reviews, 134: 98-136.
Li, J., Shi, W., Zhang, Y., Dong, S., Ma, Z. 2016a. Thermal evolution of the Hengshan extensional dome in central South China and its tectonic implications: New insights into low-angle detachment formation. Gondwana Research, 35: 425-441.
Li, J., Dong, S., Zhang, Y., Zhao, G., Johnston, S. T., Cui, J., Xin, Y. 2016b. New insights into Phanerozoic tectonics of south China: Part 1, polyphase deformation in the Jiuling and Lianyunshan domains of the central Jiangnan Orogen. Journal of Geophysical Research: Solid Earth, 121(4): 3048-3080.
Li, Y., Zheng, D., Wu, Y., Wang, Y., He, H., Pang, J., Yu, J. 2017. A potential (U- Th)/He zircon reference material from Penglai zircon megacrysts. Geostandards and Geoanalytical Research, 41(3): 359-365.
Li, W., Liu, S., Wang, Y., Qian, T., Gao, T. 2017. Duplex thrusting in the South Dabashan arcuate belt, central China. Journal of Structural Geology, 103: 120-136.
Li, Y., He, D., Li, D., Lu, R., Fan, C., Sun, Y., Huang, H. 2018. Sedimentary provenance constraints on the Jurassic to Cretaceous paleogeography of Sichuan Basin, SW China. Gondwana Research, 60: 15-33.
Li, J., Dong, S., Cawood, P. A., Zhao, G., Johnston, S. T., Zhang, Y., Xin, Y. 2018. An Andean-type retro-arc foreland system beneath northwest South China revealed by SINOPROBE profiling. Earth and Planetary Science Letters, 490: 170-179.
Li, S., Suo, Y., Li, X., Zhou, J., Santosh, M., Wang, P., Zhang, G. 2019. Mesozoic tectono-magmatic response in the East Asian ocean-continent connection zone to subduction of the Paleo-Pacific Plate. Earth-Science Reviews, 192: 91-137.
Lin, W., Faure, M., Monié, P., Schärer, U., Zhang, L., Sun, Y. 2000. Tectonics of SE China: new insights from the Lushan massif (Jiangxi Province). Tectonics, 19(5): 852-871.
Lin, X., Jolivet, M., Liu-Zeng, J., Cheng, F., Tian, Y., Li, C. 2021. Mesozoic-Cenozoic cooling history of the Eastern Qinghai Nan Shan (NW China): Apatite low-temperature thermochronology constraints. Palaeogeography, Palaeoclimatology, Palaeoecology, 572: 110416.
Lin, X., Li, L., Liu, J., L, Ch. Liu, H. 2022a. The Yangtze River contributed detrital materials to the Jianghan Basin during the Early Pleistocene: Constraints from detrital zircon U-Pb ages. Journal of Earth Science, 0(0): 1-13(in Chinese with English abstract).
Lin, X., Jolivet, M., Liu-Zeng, J., Cheng, F., Wu, Z., Tian, Y., Chen, J. 2022b. The formation of the North Qilian Shan through time: Clues from detrital zircon fission-track data from modern river sediments. Geosciences, 12(4), 166: 1-20.
Lin, X., Liu-Zeng, J., Jolivet, M., Liu, W., Liu, H. 2023a. Sedimentary provenance constraints on the Cretaceous to Cenozoic palaeogeography of the western margin of the Jianhan Basin, South China. Gondwana Research, in press.
Lin, X., Jolivet, M., Cheng, F. 2023b. Spatiotemporal evolution of Central Qilian Shan (Northwest China): Constrained by fission-track ages of detrital grains from the Huangshui River. Minerals, 13(7):1-13.
Liu, S., Heller, P. L., Zhang, G. 2003. Mesozoic basin development and tectonic evolution of the Dabieshan orogenic belt, central China. Tectonics, 22(4): 1-21.
Liu, S., Steel, R., Zhang, G. 2005. Mesozoic sedimentary basin development and tectonic implication, northern Yangtze Block, eastern China: record of continent–continent collision. Journal of Asian Earth Sciences, 25(1): 9-27.
Liu, S., Qian, T., Li, W., Dou, G., Wu, P. 2015a. Oblique closure of the northeastern Paleo-Tethys in central China. Tectonics, 34(3): 413-434.
Liu, S., Li, W., Wang, K., Qian, T., Jiang, C. 2015b. Late Mesozoic development of the southern Qinling-Dabieshan foreland fold-thrust belt, Central China, and its role in continent-continent collision. Tectonophysics, 644: 220-234.
Liu, S., Gurnis, M., Ma, P., Zhang, B. 2017. Reconstruction of northeast Asian deformation integrated with western Pacific plate subduction since 200 Ma. Earth-Science Reviews, 175: 114-142.
Liu, S., Yang, Y., Deng, B., Zhong, Y., Wen, L., Sun, W., Peng, H. 2021. Tectonic evolution of the Sichuan basin, southwest China. Earth-Science Reviews, 213, 103470.
Liu, Y., Liu, X., Wang, S., Xu, S., Ellam, R. M., Fabel, D., Chen, J. 2022. Late Cenozoic channel migration of the proto-Yangtze River in the delta region: Insights from cosmogenic nuclide burial dating of onshore boreholes. Geomorphology, 407: 108228.
Liu-Zeng, J., Zhang, J., McPhillips, D., Reiners, P., Wang, W., Pik, R., Ge, Y. 2018. Multiple episodes of fast exhumation since Cretaceous in southeast Tibet, revealed by low-temperature thermochronology. Earth and Planetary Science Letters, 490: 62-76.
Ludwig, K. R. 2003. User's manual for IsoPlot 3.0. A geochronological toolkit for Microsoft Excel, 71.
McPhillips, D., Hoke, G. D., Liu-Zeng, J., Bierman, P. R., Rood, D. H., Niedermann, S. 2016. Dating the incision of the Yangtze River gorge at the First Bend using three- nuclide burial ages. Geophysical Research Letters, 43(1): 101-110.

Pang, J., Zheng, D., Ma, Y., Wang, Y., Wu, Y., Wan, J., Wang, Y. 2017. Combined apatite fission-track dating, chlorine and REE content analysis by LA-ICPMS. Science Bulletin, 62(22): 1497-1500.
Ratschbacher, L., Hacker, B. R., Webb, L. E., McWilliams, M., Ireland, T., Dong, S., Wenk, H. R. 2000. Exhumation of the ultrahigh- pressure continental crust in east central China: Cretaceous and Cenozoic unroofing and the Tan- Lu fault. Journal of geophysical research: Solid Earth, 105(B6): 13303-13338.
Reiners, P. W., Farley, K. A. 2001. Influence of crystal size on apatite (U–Th)/He thermochronology: an example from the Bighorn Mountains, Wyoming. Earth and Planetary Science Letters, 188(3-4): 413-420.
Reiners, P. W., Farley, K. A., Hickes, H. J. 2002. He diffusion and (U–Th)/He thermochronometry of zircon: initial results from Fish Canyon Tuff and Gold Butte. Tectonophysics, 349(1-4): 297-308.
Reiners, P. W., Brandon, M. T. 2006. Using thermochronology to understand orogenic erosion. Annu. Rev. Earth Planet. Sci., 34, 419-466.
Richardson, N. J., Densmore, A. L., Seward, D., Wipf, M., Yong, L. 2010. Did incision of the Three Gorges begin in the Eocene?. Geology, 38(6): 551-554.
Shen, Y. C. 1965. Geomorphology of the upper Yangtze River Valley. Beijing: Geological Publishing House, 1-162 (in Chinese with English abstract).
Shen, C., Mei, L., Peng, L., Chen, Y., Yang, Z., Hong, G. 2012a. LA-ICPMS U–Pb zircon age constraints on the provenance of Cretaceous sediments in the Yichang area of the Jianghan Basin, central China. Cretaceous Research, 34: 172-183.
Shen, C., Donelick, R. A., O'Sullivan, P. B., Jonckheere, R., Yang, Z., She, Z. B., Ge, X. 2012b. Provenance and hinterland exhumation from LA-ICP-MS zircon U–Pb and fission-track double dating of Cretaceous sediments in the Jianghan Basin, Yangtze block, central China. Sedimentary Geology, 281: 194-207.
Shen, C., Hu, D., Min, K., Yang, C., Zeng, X., Fu, H., Ge, X. 2020. Post-Orogenic tectonic evolution of the Jiangnan-Xuefeng orogenic belt: Insights from multiple geochronometric dating of the Mufushan Massif, South China. Journal of Earth Science, 31: 905-918.
Shi, W., Zhang, Y., Dong, S., Hu, J., Wiesinger, M., Ratschbacher, L., Li, H. 2012. Intra-continental Dabashan orocline, southwestern Qinling, central China. Journal of Asian Earth Sciences, 46: 20-38.
Shi, W., Dong, S. W., Ratschbacher, L., Tian, M., Li, J. H., Wu, G. L. 2013. Meso-Cenozoic tectonic evolution of the Dangyang Basin, north-central Yangtze craton, central China. International Geology Review, 55(3): 382-396.
Shi, W., Dong, S., Zhang, Y., Huang, S. 2015. The typical large-scale superposed folds in the central South China: Implications for Mesozoic intracontinental deformation of the South China Block. Tectonophysics, 664: 50-66.
Shi, H., Shi, X., Glasmacher, U. A., Yang, X., Stockli, D. F. 2016. The evolution of eastern Sichuan basin, Yangtze block since Cretaceous: constraints from low temperature thermochronology. Journal of Asian Earth Sciences, 116: 208-221.
Shuster, D. L., Flowers, R. M., Farley, K. A. 2006. The influence of natural radiation damage on helium diffusion kinetics in apatite. Earth and Planetary Science Letters, 249(3-4): 148-161.
Tang, S. L., Yan, D. P., Qiu, L., Gao, J. F., Wang, C. L. 2014. Partitioning of the Cretaceous Pan-Yangtze Basin in the central South China Block by exhumation of the Xuefeng Mountains during a transition from extensional to compressional tectonics?. Gondwana Research, 25(4): 1644-1659.
Tian, Y., Qiu, N., Kohn, B. P., Zhu, C., Hu, S., Gleadow, A. J., McInnes, B. I. 2012. Detrital zircon (U–Th)/He thermochronometry of the Mesozoic Daba Shan Foreland Basin, central China: Evidence for timing of post-orogenic denudation. Tectonophysics, 570: 65-77.
Tian, Y., Kohn, B. P., Hu, S., Gleadow, A. J. 2015. Synchronous fluvial response to surface uplift in the eastern Tibetan Plateau: Implications for crustal dynamics. Geophysical Research Letters, 42(1): 29-35.
Vermeesch, P. 2009. RadialPlotter: A Java application for fission track, luminescence and other radial plots. Radiation Measurements, 44(4): 409-410.
Vermeesch, P., Tian, Y. 2014. Thermal history modelling: HeFTy vs. QTQt. Earth-Science Reviews, 139: 279-290.
Wang, P., Liu, Sh., Zheng, H., Wang, Kai, Gao, T., Pan, F., Li, W., Jiang, Ch., Chen, Y., Yang, X. 2012. Late-orogenic arcuate fold-thrust belts in northern Yangtze area:Structural characteristics and basin evolution. Journal of Palaeogeography, 15(6): 819-838 (in Chines with English abstract).
Wang, P., Zheng, H., Liu, S. 2013. Geomorphic constraints on middle Yangtze River reversal in eastern Sichuan Basin, China. Journal of Asian Earth Sciences, 69: 70-85.
Wang, P., Zheng, H., Chen, L., Chen, J., Xu, Y., Wei, X., Yao, X. 2014. Exhumation of the Huangling anticline in the Three Gorges region: Cenozoic sedimentary record from the western Jianghan Basin, China. Basin Research, 26: 505-522.
Wang, F., Zhu, R., Hou, Q., Zheng, D., Yang, L., Wu, L., Liu, Q. 2015. 40Ar/39Ar Thermochronology on Central China Orogen: Cooling, uplift and implications for orogeny dynamics. Geological Society, London, Special Publications, 378(1): 189-206.
Wang, P., Zheng, H., Liu, S., Hoke, G. 2018. Late Cretaceous drainage reorganization of the middle Yangtze River. Lithosphere, 10(3): 392-405.
Wang, M., Tian, Y., Zhou, B., Jiao, R., Zhang, G. 2022. Instant far-field effects of continental collision: An example study in the Qinling Orogen, northeast of the Tibetan Plateau. Tectonophysics, 833: 229334.
Wang, L., Ding, L., Garzanti, E., Shen, L., Nulay, P., Siritongkham, N. 2022. Mid-Cretaceous drainage reorganization and exorheic to endorheic transition in Southeast Tibet. Sedimentary Geology, 439: 106221.
Wang, L., Malkowski, M. A., Cai, F., Shen, L., Saboor, A., Liu, C., Ding, L. 2023. A climate-driven transcontinental drainage system in the southeast Tibetan Plateau during the Early Cretaceous. Journal of Asian Earth Sciences, 105615.
Wissink, G. K., Hoke, G. D., Garzione, C. N., Liu- Zeng, J. 2016. Temporal and spatial patterns of sediment routing across the southeast margin of the Tibetan Plateau: Insights from detrital zircon. Tectonics, 35(11): 2538-2563.
Yang, D.Y. 2006. Geomorphic process of Yangtze River. Beijing: Geological Publishing House, 1-219 (in Chinese with English abstract).
Yang, Z., Shen, C., Ratschbacher, L., Enkelmann, E., Jonckheere, R., Wauschkuhn, B., Dong, Y. 2017. Sichuan Basin and beyond: Eastward foreland growth of the Tibetan Plateau from an integration of Late Cretaceous-Cenozoic fission track and (U-Th)/He ages of the eastern Tibetan Plateau, Qinling, and Daba Shan. Journal of Geophysical Research: Solid Earth, 122(6): 4712-4740.
Yu, J., Zheng, D., Pang, J., Wang, Y., Fox, M., Vermeesch, P., Wang, Y. 2019. Miocene range growth along the Altyn Tagh Fault: Insights from apatite fission track and (U-Th)/He thermochronometry in the western Danghenan Shan, China. Journal of Geophysical Research: Solid Earth, 124(8): 9433-9453.

Yuan, J., Yang, Z., Deng, C., Krijgsman, W., Hu, X., Li, S., Zhu, R. 2021. Rapid drift of the Tethyan Himalaya terrane before two-stage India-Asia collision. National Science Review, 8(7): 1-13.
Zhao, X., Zhang, H., Tao, Y., Wang, Y., Pang, J., Ma, Y., Xiong, J. 2021. Pliocene to Early Pleistocene drainage reorganization in eastern Tibet inferred from detrital zircons. Geophysical Research Letters, 48(20): e2021GL094563.
Zhao, X., Zhang, H., Hetzel, R., Kirby, E., Duvall, A. R., Whipple, K. X., Zhang, P. 2022. Existence of a continental-scale river system in eastern Tibet during the late Cretaceous–early Palaeogene. Nature communications, 12(1): 7231.
Zhang, S. B., Zheng, Y. F., Wu, Y. B., Zhao, Z. F., Gao, S., Wu, F. Y. 2006. Zircon U–Pb age and Hf isotope evidence for 3.8 Ga crustal remnant and episodic reworking of Archean crust in South China. Earth and Planetary Science Letters, 252(1-2): 56-71.
Zhang, Y., Li, C. A., Wang, Q., Chen, L., Ma, Y., Kang, C. 2008. Magnetism parameters characteristics of drilling deposits in Jianghan Plain and indication for forming of the Yangtze River Three Gorges. Science Bulletin, 53(4): 584-590.
Zhang, Z., Shen, C., Shao, C., Liu, Z. 2013. Tectonothermal evolution of the eastern Tibetan Plateau Foreland: fission-track thermochronology of the southern Dabashan Fold-Thrust Belt. Journal of Earth Science, 24(4): 479-490.
Zhang, B., Liu, S., Wan, N., Xu, Q. 2023. Paleostress regime evolution in South China induced by dynamic changes in Izanagi-Pacific subduction since the Cretaceous. Journal of Structural Geology, 104934.
Zheng, H., Clift, P. D., Wang, P., Tada, R., Jia, J., He, M., Jourdan, F. 2013. Pre-miocene birth of the Yangtze River. Proceedings of the National Academy of Sciences, 110(19): 7556-7561.
Zhou, X., Sun, T., Shen, W., Shu, L., Niu, Y. 2006. Petrogenesis of Mesozoic granitoids and volcanic rocks in South China: a response to tectonic evolution. Episodes Journal of International Geoscience, 29(1): 26-33.
Zhu, D. C., Zhao, Z. D., Niu, Y., Dilek, Y., Hou, Z. Q., Mo, X. X. 2013. The origin and pre-Cenozoic evolution of the Tibetan Plateau. Gondwana Research, 23(4): 1429-1454.

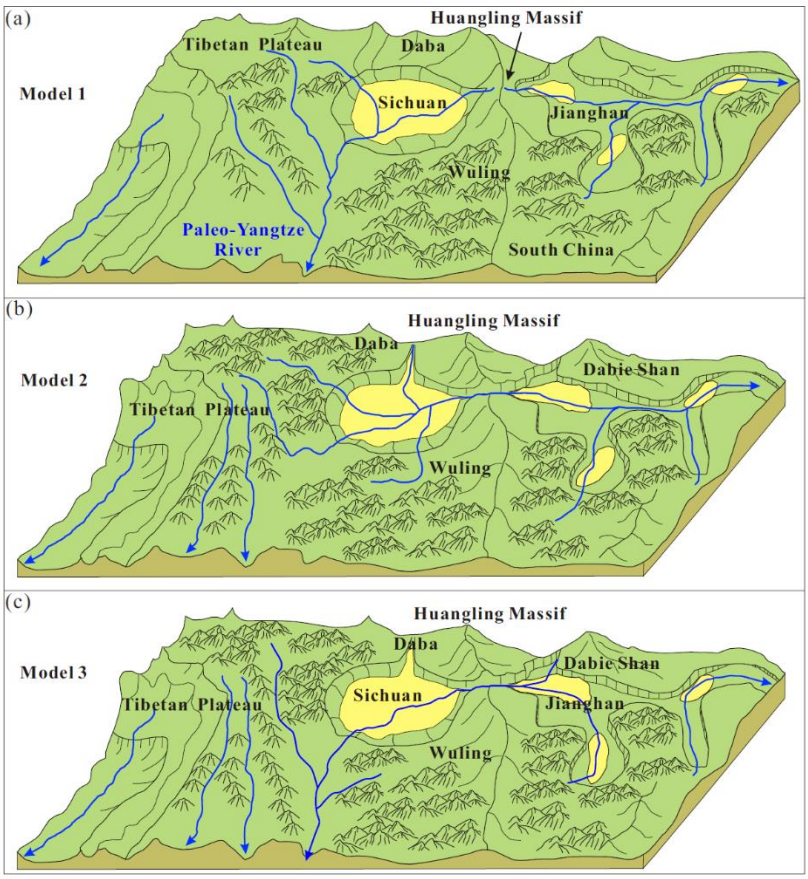

Fig. 1. Evolution model of the Yangtze River near the Huangling Massif during the Cretaceous. (a) Model 1: The Huangling Massif becomes a watershed with rivers flowing into the Sichuan and Jianghan Basins on both sides (Lee, 1924; Yang, 2006; Deng et al., 2018); (b) Model 2: The Yangtze River flows through the Huangling Massif from west to east (Lee, 1934; Barbour, 1936; Shen, 1965); (c) Model 3: The Yangtze River flows through the Huangling Massif from east to west (Wang et al., 2018).

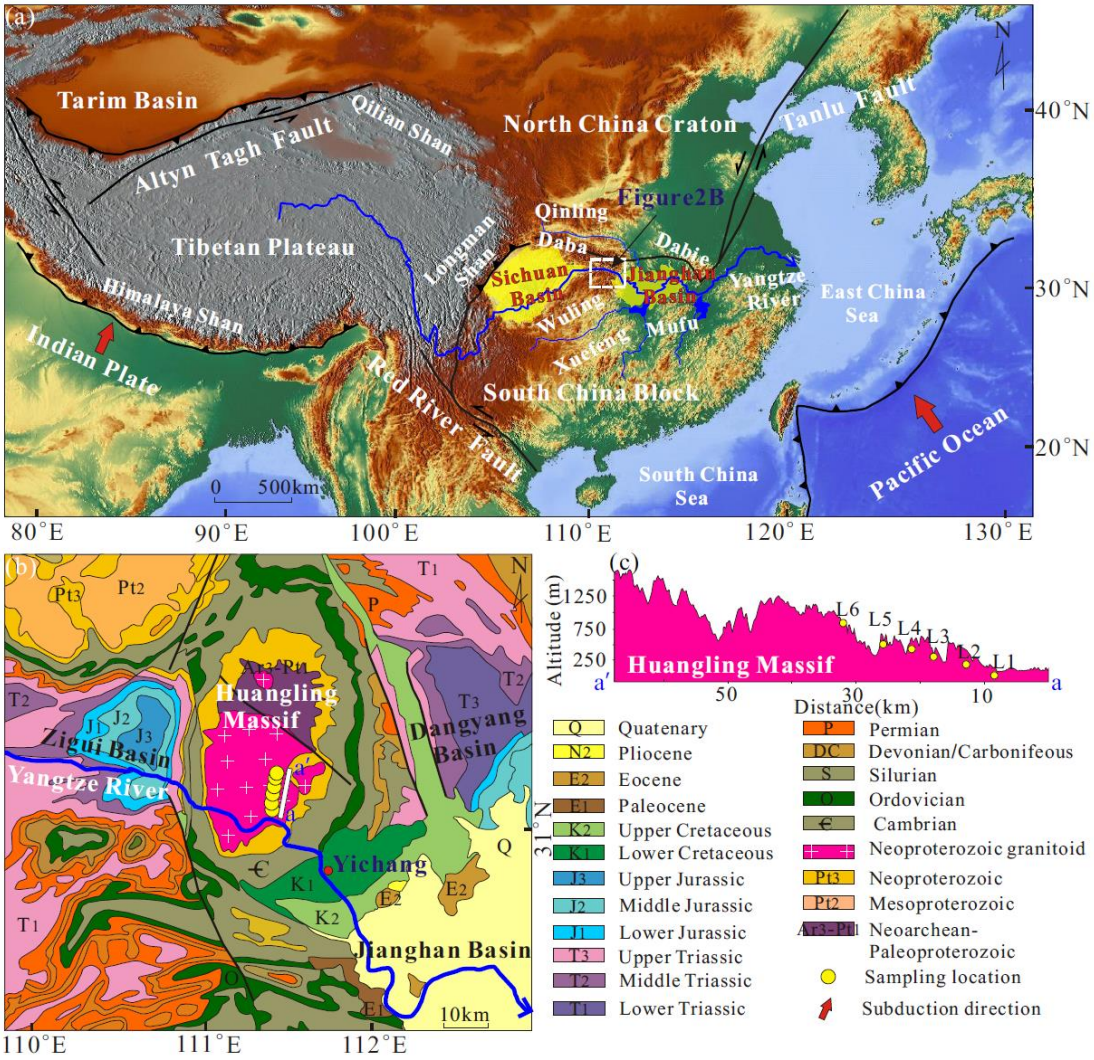

Fig. 2. (a) Location of the Huangling Massif and its surrounding major tectonic units (modified from Li et al., 2014); (b) geologic map of the Huangling Massif (modified from Hubei BGMR, 1970), with a–a' representing the sampling locations; (c) cross-sectional diagram of sampling locations, with yellow circles representing sampling locations.

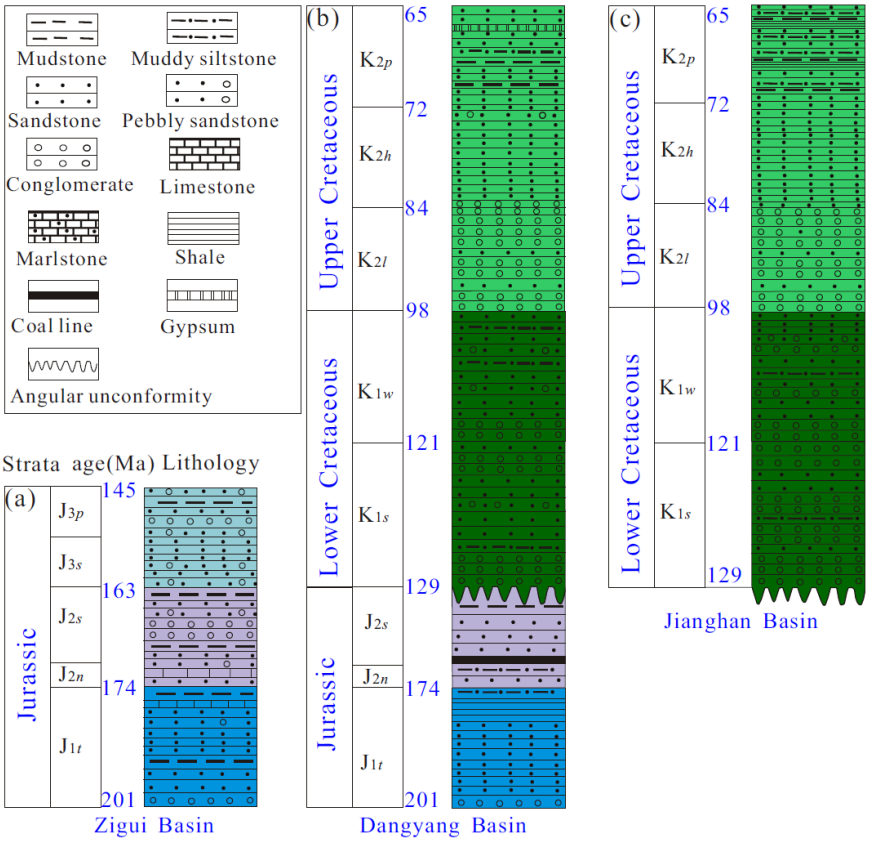

Fig. 3. Geological stratigraphic columns (Hubei BGMR, 1990). (a) Zigui Basin; (b) Dangyang Basin; (c) Jianghan Basin.

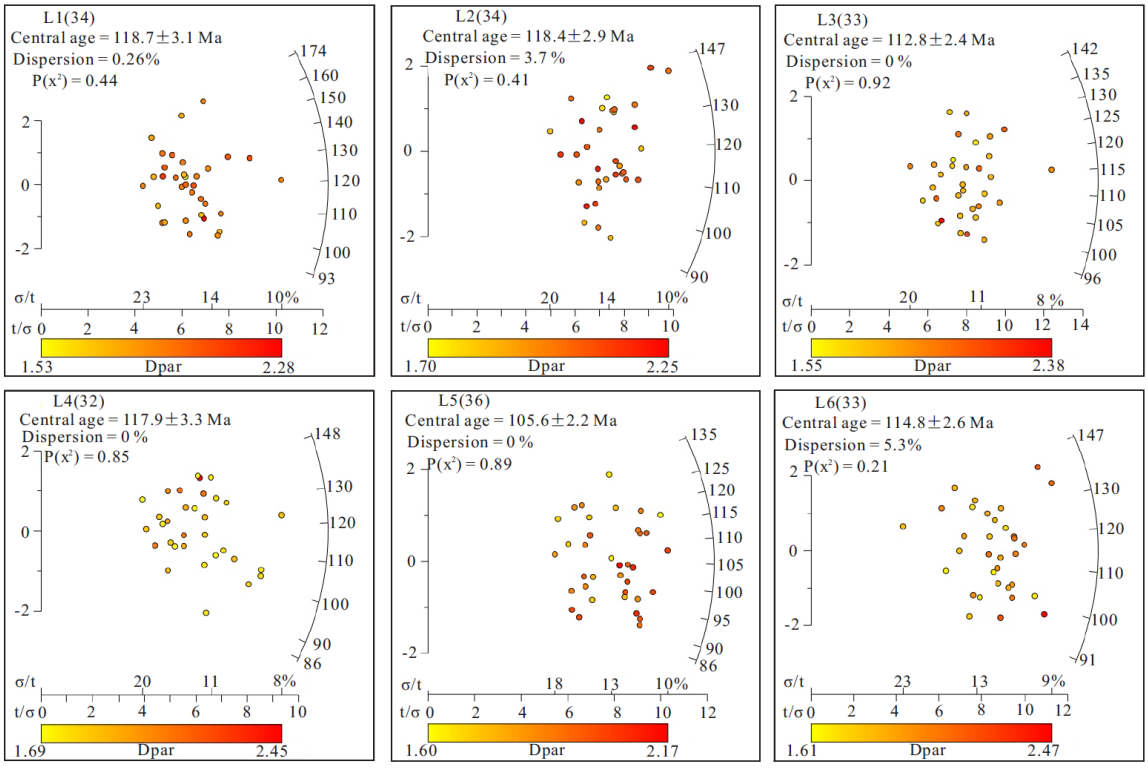

Fig. 4. Radial plots for apatite fission-track ages from the Huangling Massif generated using the RadialPlotter software (Vermeesch, 2009).

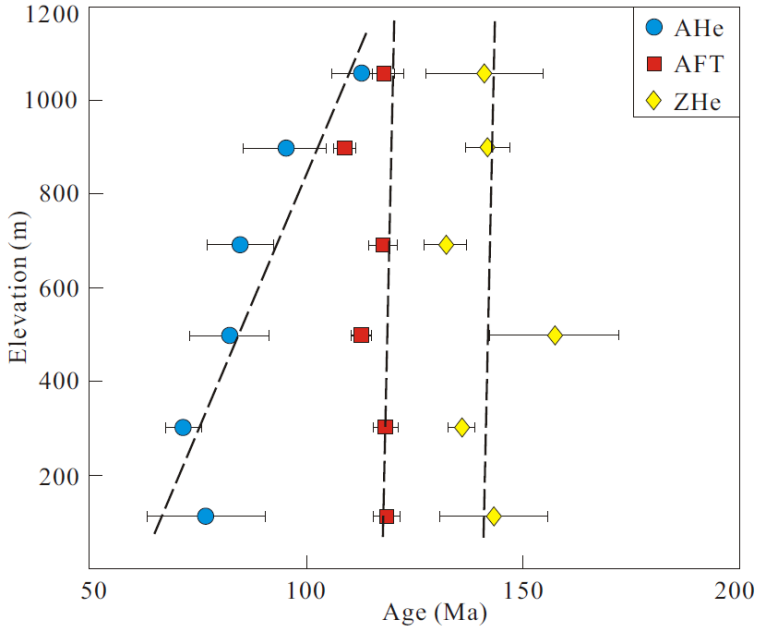

Fig. 5. Apatite and zircon (U–Th)/He and apatite fission track cooling ages corresponding to elevations for the Huangling Massif. The AHe ages show a broadly positive correlation with the elevations. The black dashed lines show age–elevation trends.

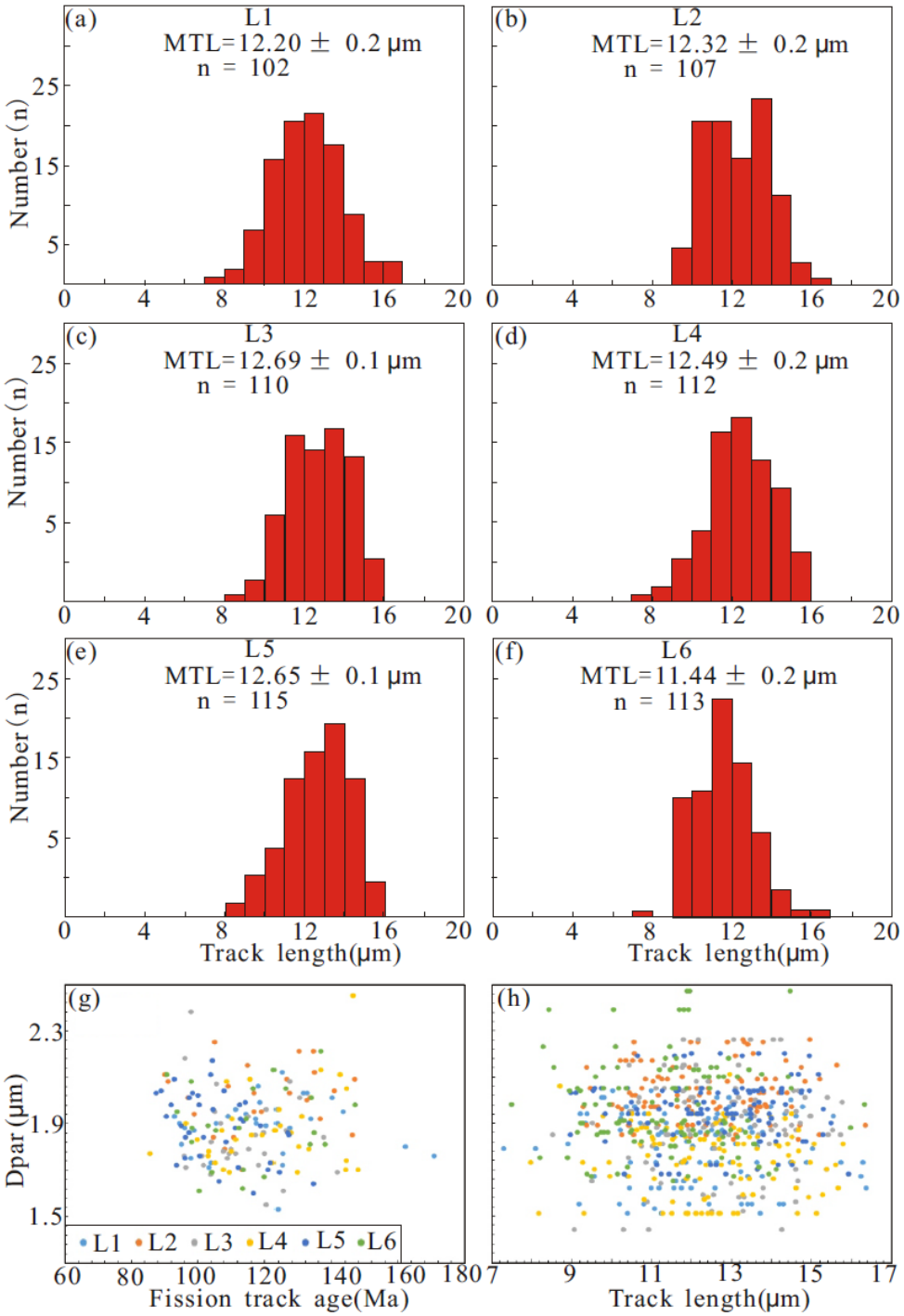

Fig. 6. (a–f) Apatite track length distribution belonging to a unimodal distribution pattern (Gleadow et al., 1986); plots of (g) apatite fission-track age and (h) track length versus Dpar.

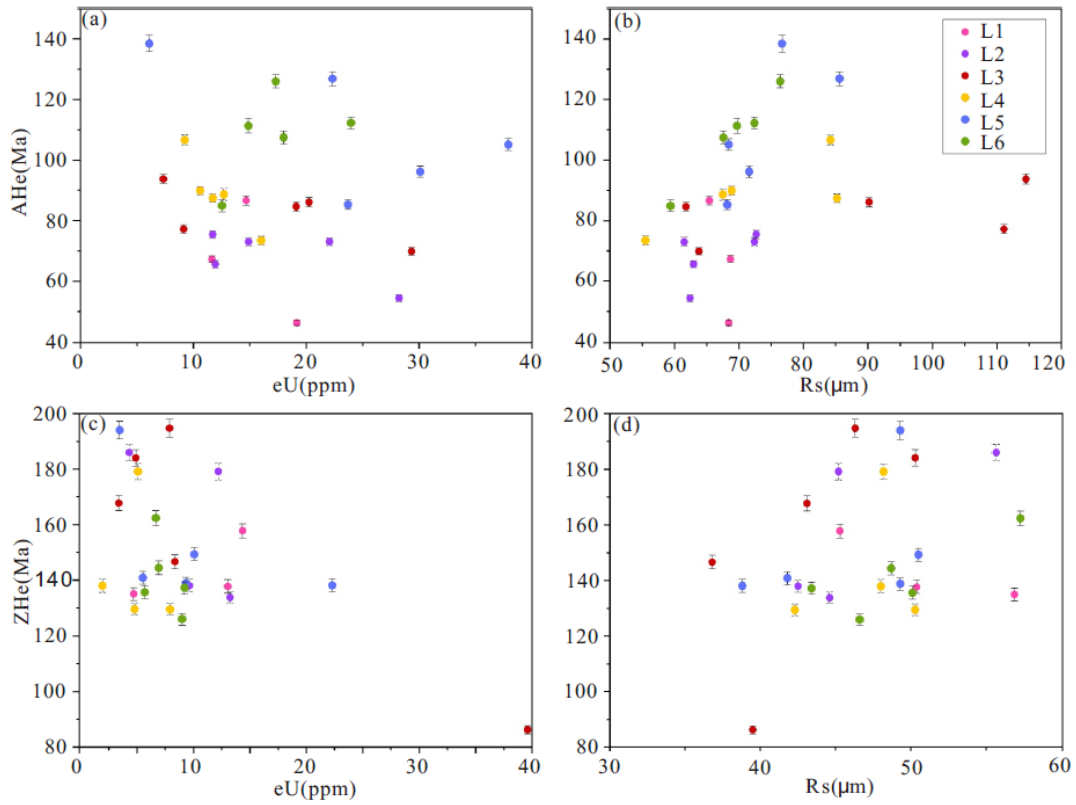

Fig. 7. Plots of (a, b) apatite and (c, d) zircon (U–Th)/He ages versus the effective U concentration (eU) and sphere equivalent radius (Rs).

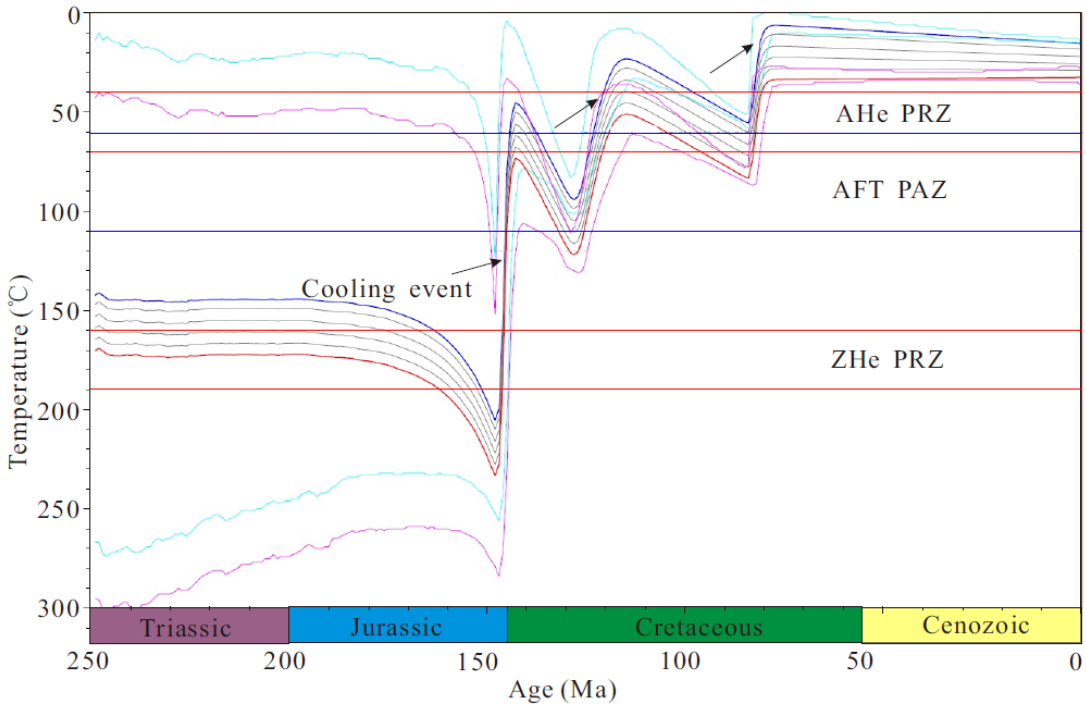

Fig. 8. Composite thermal histories for samples from the Huangling Massif showing that major cooling/exhumation events (black arrows) occurred in the Late Jurassic–Early Cretaceous, as well as late Early Cretaceous and Late Cretaceous. ZHe PRZ: zircon (U–Th)/He partial retention zone; AFT: apatite fission track partial annealing zone; AHe PRZ: apatite (U–Th)/He partial retention zone.

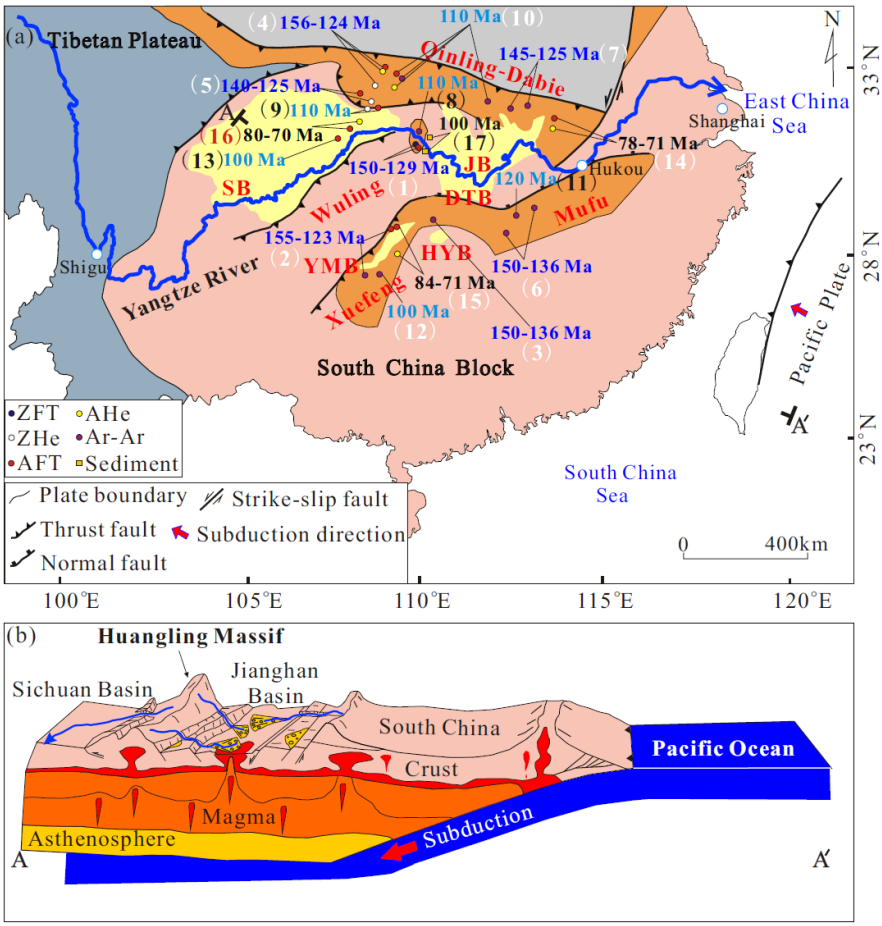

Fig. 9. (a) Sketch map showing the cooling ages and distributions from the South China Block. (1): Ge et al. (2013); (2): Ge et al. (2016); Chu et al. (2019); (3): Li et al. (2013, 2016a); (4): Heberer et al. (2014); Chen et al. (2015); Wang M et al. (2022); (5): Shi et al. (2012); Tian et al. (2012); Zhang et al. (2013); (6): Li et al. (2016); Ji et al. (2017a); Shen et al. (2020); (7): Ratschbacher et al. (2000); Grimmer et al. (2002); Hu et al. (2006b); Ji et al. (2017b); (8): Ji et al. (2014); (9): Tian et al. (2012); Li W et al. (2017); (10): Grimmer et al. (2002); Heberer et al. (2014); Wang et al. (2015); Wang M et al. (2022); (11): Shen et al. (2020); (12): Chu et al. (2020); (13): Shi et al. (2016); (14): Chen et al. (2015); Ding et al. (2021); (15): Tang et al. (2014); Ge et al. (2016); (16): Deng et al. (2013); Shi et al. (2016); Yang et al. (2017); (17): Shi et al. (2013); Shen et al. (2012b); (b) illustration showing the subduction of the Pacific Plate beneath the South China Block during the Cretaceous (modified from Li et al. (2014) and Chu et al.(2020)). The Huangling Massif was affected by the subduction and finally became the watershed between the Sichuan and Jianghan Basins.

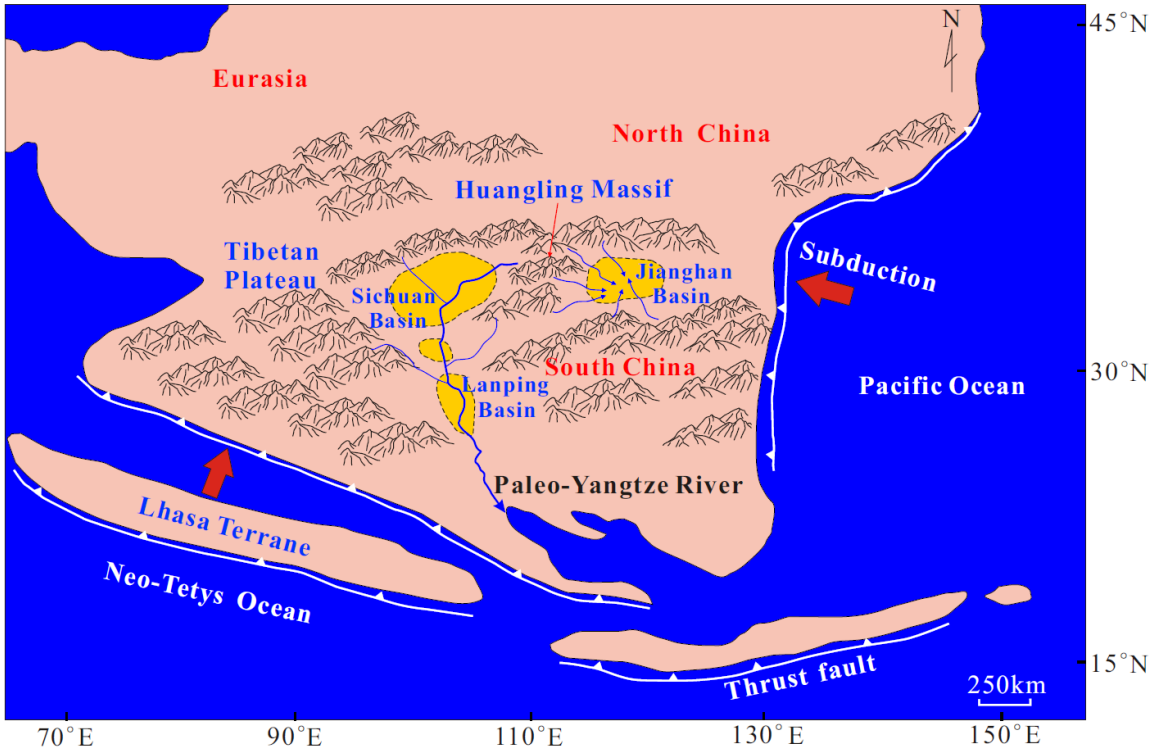

Fig. 10. Reconstruction map of the flow direction of the Paleo-Yangtze River in the Late Mesozoic from the South China Block (Shen et al., 2012a; Deng et al., 2018; Lin et al., 2023a; Wang et al., 2023). Influenced by the subduction of the Pacific Plate and Lhasa Terrane beneath the Asian continent, the Paleo-Yangtze River flowed between the Tibetan Plateau and South China Block (Plateau).

About the first author

SU Jianchao, male, born in 1992 in Xinxiang City, Henan Province. Doctoral of China University of Geosciences (Wuhan). His primary research interests focus on the evolutionary processes of the Three Gorges of the Yangtze River and provenance tracing in the Jianghan Basin. E-mail: Alan1cug@163.com.

About the corresponding authors

LIN Xu, male, born in 1984 in Weihai City, Shandong Province; Ph.D., Quaternary geology, China Three Gorges University. He is currently devoted to studying the evolutionary processes of the Three Gorges of the Yangtze River, the uplift of the Tibetan Plateau specifically focusing on the Qilian Mountains, and the evolution of the Yellow River. E-mail: hanwuji-life@163.com.

LI Chang'an, male, born in 1958 in Handan City, Hebei Province; Ph.D., Quaternary geology, China University of Geosciences (Wuhan). His research interests include river geomorphic processes, Quaternary geology and environment, and sustainable development. E-mail: 1002858465@qq.com.